Nanomed. J. 7(4): 272-283, Autumn 2020

RESEARCH PAPER

Comparative antimicrobial and anticancer activity of biologically and chemically synthesized zinc oxide nanoparticles toward breast cancer cells

Karthigadevi Guruviah [1*], Sathish Kumar Annamalai [2,3], Arulvel Ramaswamy [1], Chozhavendhan Sivasankaran [4], Subbaiya Ramasamy [5], Hamed Barabadi [6], Muthupandian Saravanan [7**]

[1]Department of Biotechnology, Saveetha School of Engineering, Saveetha Institute of Medical and Technical Sciences, Saveetha Nagar, Thandalam, Chennai – 602 105
[2]Hubert Enviro Care Systems (P) Ltd., Thiru Vi Ka Industrial Estate, Guindy, Chennai–600 032, Tamil Nadu, India
[3]Department of Biotechnology, Sree Sastha Institute of Engineering and Technology, Chennai–600 123, Tamil Nadu, India
[4]Department of Biotechnology, Vivekanandha College of Engineering for Women, Elayampalayam, Tiruchengode – 637 210, Namakkal, Tamil Nadu, India
[5]Department of Biological Sciences, School of Mathematics and Natural Sciences, The Copperbelt University, Riverside, Jambo Drive, P.O. Box. 21692, Kitwe, Zambia
[6]Department of Pharmaceutical Biotechnology, School of Pharmacy, Shahid Beheshti University of Medical Sciences, Tehran, Iran
[7] Department of Microbiology and Immunology, Division of Biomedical Sciences, School of Medicine, College of Health Sciences, Mekelle University, Mekelle-1871, Ethiopia

ABSTRACT

Objective(s): This study was aimed to investigate the synthesis of novel zinc oxide (ZnO) nanoparticles (NPs) using Solanum trilobatum leaf extract as the reducing and capping agents, called green synthesized zinc oxide nanoparticles (GS-ZnONPs).

Materials and Methods: Chemically synthesized zinc oxide nanoparticles (CS-ZnONPs) were synthesized using precipitation method with zinc nitrates hexahydrate as reducing precursors. The synthesized GS- and CS-ZnONPs were examined and characterized using UV-visible spectroscopy, Transmission Electron Microscopy (TEM), Scanning Electron microscopy (SEM), Energy dispersive X-ray analysis (EDAX), and X-ray diffraction (XRD) analysis, respectively.

Results: GS-ZnONPs exhibited a higher zone of inhibition of 28.6 mm, 27.63 mm, and 29.33 mm for Bacillus subtilis, Escherichia coli, and Klebsiella pneumoniae, respectively compared to CS-ZnONPs. From the growth inhibition experiments with E. coli and Staphylococcus aureus, it was evident that GS-ZnONPs have exhibited higher growth inhibition as compared to CS-ZnONPs. The IC50 for CS-ZnONPs in MCF-7 cell line was found at 136.16 µg/mL and for GS-ZnONPs was found at 85.05 µg/mL. The proliferation of cancer cells were directly proportional to the concentration of NPs. As compared to CS-ZnONPs, GS-ZnONPs have exhibited higher cytotoxic effects on MCF-7 cell line.

Conclusion: It was concluded that GS-ZnONPs represented much enhanced anticancer and antibacterial activity compared to CS-ZnONPs.

Keywords: *Antimicrobial, Breast cancer, Cytotoxicity, Zinc oxide nanoparticles*

How to cite this article
Guruviah K, Kumar Annamalai S, Ramaswamy A, Sivasankaran Ch, Ramasamy S, Barabadi H, Saravanan M. Comparative antimicrobial and anticancer activity of biologically and chemically synthesized zinc oxide nanoparticles toward breast cancer cells. Nanomed J. 2020; 7(4):272-283. DOI: 10.22038/nmj.2020.07.00003

* *Corresponding Author Email: devigk19@gmail.com, bioinfosaran@gmail.com, saravanan.muthupandian@mu.edu.et*
Note. This manuscript was submitted on May 1, 2020; approved on August 10, 2020

INTRODUCTION

Nanotechnology researches are the priority field and the forefront of modern research in recent years in different sciences such as, medicine, physics, chemistry, biology, etc [1, 2]. Nanomaterials with its unique physical and chemical properties supported by various applications by changing their size, distribution, and morphology [3]. Multiple methodologies were developed in this field to synthesize biocompatible NPs to meet the specific needs, mainly in the applications related to the medicinal field. Metal NPs have recently attracted significant attraction due to their particular morphologies which are account for numerous applications [4]. ZnO is a naturally existing metal in the earth crust as a non-toxic mineral. ZnO is a multifunctional element that exhibits new and improved properties by controlling their physical and chemical properties [5]. Nanomaterials based on ZnO exhibit various applications mainly as energy storage devices, optical devices, and nano-sensors [6-8]. The critical feature of the ZnONPs is that they are rich in hydroxyl groups which provide space for functionalization [9]. It also possesses less toxicity, high biodegradability which gain importance in biomedical applications [10]. ZnONPs can be synthesize with different mechanochemical, chemical and biological methods. The mechanochemical methods included laser ablation and high-energy ball milling techniques [11, 12]. Pyrolysis byproducts resulting from laser ablation method is a significant disadvantage of the laser ablation technique [13]. Besides, contamination from milling balls is the major disadvantage of the high-energy ball milling technique [14, 15]. Moreover, the chemical methods such as co-precipitation, sol-gel, and hydrothermal techniques have been used for the synthesis of ZnONPs [11, 12]. Trace impurity and time consuming are the drawbacks of co-precipitation technique [12]. Besides, shrinkage and cracking during drying and expensive raw materials are some of the disadvantages of sol–gel technique [16]. Moreover, slow reaction kinetics [17] and the need for expensive autoclaves [18] are the drawbacks of hydrothermal technique for preparation of NPs. Hence, there is a growing need for a simple, fast and eco-friendly method to synthesized ZnONPs. Plant extracts-based nanoparticle synthesis becomes more attractive as they eliminate the use of hazardous chemicals for the synthesis process. *S. trilobatum* Linn belongs to the *Solanaceae* family and is a prominent Indian medicinal plant. It is commonly known as 'Thuthuvalai' in Tamil. The leaves of the plants were utilized for curing a common cold, asthma, and tuberculosis [19]. Moreover, it was prescribed to various other diseases in Ayurveda and Siddha medicinal systems [19-23]. The phytochemical analysis of the plant has revealed the presence of alkaloids such as soladunalinidine, tomatidine [24], sobatum [19], β-solamarine, solasodine [25], and solaine. It possesses excellent antioxidant and hepatoprotective properties [26]. In this study, we have mainly focused on the optimization of both the chemical and green synthesized ZnONPs from the leaves of thorny creeper *Solanum* and its characterization and their application as an antimicrobial and anticancer agent.

MATERIALS AND METHODS

Synthesis of ZnO nanoparticles (ZnONPs)

Chemical synthesis–precipitation method

The utilized chemicals were of analytical grade obtained from Fisher chemical (India), Mumbai. Zinc nitrate hexahydrate ($Zn(NO_3)_2$ $6H_2O$) and ammonium carbonate ((NH4)2CO3) were used as a precursor and doping agent to synthesize ZnONPs via direct precipitation method [27].

Briefly, 1.0 M of zinc nitrate hexahydrate (100 mL) was slowly dropped on to vigorously stirred (400 rpm and 28 ºC) solution with the molar ratio of 1:1.5 (1.0 mM of ammonium carbonate (150 mL)). The addition of zinc nitrate hexahydrate and ammonium carbonate solution resulted in the formation of white precipitate. The precipitate was collected through filtration using filter paper (Whatman® quantitative filter paper, ash less, Grade 41), and the filtrate was washed thrice with distilled water and 70% ethanol. The precipitate was collected and dried at 100 ºC for six hours to form ZnO precursor. The ZnO precursor was galvanized in the muffle furnace at the temperature of 550 ºC for 4 h [28].

Green Synthesis of ZnONPs using S. trilobatum

Collection of plant material

S. trilobatum leaves of the same age group of single inhabitants were collected from the Tamil Nadu medicinal plant farms, and herbal medicine corporation limited, Anna Hospital Campus, Chennai, Tamil Nadu. *S. trilobatum* leaves were utilized as the herbal source for green nanoparticle

synthesis. The Taxonomic identification of the collected plants was done at the Botanical Survey of India, Southern Regional Center, Coimbatore, Tamil Nadu. The collected leaves were transported to the laboratory; fresh and healthy leaves were separated, washed, and rinsed with tap water. The leaves of *S. trilobatum* were washed with distilled water to remove the dirt and grime and further washed with the Hiclean (Liquid soap) and rinsed thrice with deionized water. The leaves were blotted with blotting paper and shade dried at room temperature to preserve the phytochemicals for two weeks. Ensuring complete drying, the leaves were cut into tiny pieces and powdered finely by applying an electric blender, and the debris was sieved and stored in the airtight container, sieved and stored in the cool place of the airtight container until further studies [29, 30].

Preparation of aqueous extract

The leaf extract was obtained by boiling 20 g of the powdered leaf in 100 mL distilled water for 10 minutes. The extract was cooled, filtered, and stored in the dark (30 °C) using airtight containers until utilized for the study [31].

Phyto-reduction method

The green synthesis was carried out with different concentrations of plant extract, and the optimum process of the synthesis was reported below. To 50 mL of 1 M of Zn(NO3)26H2O, 25 mL of *S. trilobatum* extract was gently added dropwise under continuous stirring (250 rpm and 75 ºC) for six hours to attain colloidal complexity. The mixture was stirred until a solid particle of light greenish-yellow color was formed. At this juncture, the precipitate was washed with deionized water, and then centrifugation at 12000 rpm for 15 min [32]. The pellet was dried in a hot air oven (60 °C) for 8 h to attain the green synthesized ZnONPs [33-36].

Characterization of ZnONPs

The green synthesized and chemically synthesized ZnONPs were characterized using different techniques. For the UV–vis analysis, ZnO nano-suspension was sonicated for ten minutes, and the UV–vis spectra (Thermo Scientific, Mumbai) was recorded in the wavelength range of 200 to 800 nm [37]. The XRD studies of ZnONPs were carried out using X-ray diffractometers (Shimadzu, Kyoto, Japan) [30, 38-40]. The crystal lattice, phase structure, material identification, and the size of the ZnONPs were determined by XRD.

The surface morphology of the CS- & GS-ZnONPs was characterized by high-resolution SEM analysis (JSM-5600LV; JEOL, Tokyo, Japan). Moreover, the elemental compositions were characterized by EDAX analysis (S-3400N; Hitachi, Tokyo, Japan). Morphology and size of the sample were investigated using Hi-Resolution Transmission Electron Microscope (JEM-2100 Plus, JEOL, Tokyo, Japan).

Time-dependent growth inhibition assay

To measure and monitor the growth inhibition of *E. coli*, and *S. aureus*, new colonies were inoculated from Mueller Hinton Agar plates into 100 mL of Luria–Brentani (LB) broth (Hi-Media, Mumbai). The inoculated flasks were allowed to grow until the optical density at 600 nm reached the medium was raised to 0.1. Consequently, 2×108 CFU/mL was added to 100 mL of LB broth enhanced with 0, 0.5, 1, and 10 mM of ZnONPs and incubated in a temperature-controlled incubator cum rotary shaker (37 °C; 100 rpm). Correspondingly, the control broths of NPs were not added as the positive control. All the experiments were performed in duplicates. The optical density, which is directly proportional to the bacterial growth was determined at 600 nm using a UV–vis spectrophotometer (Thermo Scientific, Mumbai).

Antimicrobial activity of ZnONPs

The antimicrobial assay was carried out by the disk diffusion method for CS-ZnO, GS-ZnO, and *S. trilobatum* leaf extract. The cultures utilized for the study were obtained from the Microbial Type Culture Collection (MTCC), Institute of Microbial Technology (IMTECH), Chandigarh, India. The received cultures were reviewed and subcultured twice before the study. Three different concentrations of nanoparticles/plant extract (50,100 and 200 mg/mL) were investigated against *B. subtilis, E. coli,* and *K. pneumoniae*. The 6 mm sterile disks (Hi-Media. Mumbai) was loaded with 20 µL of the sample and air-dried. For positive control of antibiotic disks, Cefotaxime (30 µg), Tetracycline (30 µg) and Ampicillin (10 µg) were used against *B. subtilis, E. coli,* and *K. pneumoniae.* The zones of inhibitions were measured using the Antibiotic Zone scale (Hi-media, Mumbai) for measuring inhibition zone size in millimeter (mm).

All the assays were carried out in triplicate.

In vitro cytotoxicity assay

Human breast carcinoma (MCF7 (ATCC® HTB-22™)) cells utilized for the study was from American Type Culture Collection (ATCC, USA). The cells were cultured in DMEM/F-12 (DMEM and Ham's F-12, Gibco®, Invitrogen Cell Culture, Sigma Aldrich, Mumbai) supplemented with fetal bovine serum (10 % FBS, Sigma Aldrich, Mumbai), penicillin (100 U/mL), and streptomycin (100 µg/mL) in a 5% CO2 incubator at 37 °C. *In vitro* cytotoxicity study was determined using 3-(4,5-dimethylthiazol-2-yl)-2,5-diphenyl tetrazolium bromide (MTT) assay [41]. Briefly, 96 well plates were used at a cell density of 1 × 106 cells per 100 µL. Different concentrations of GS- and CS-ZnONPs (0, 25, 62.5, 125, 250, 500, and 1000 µg/mL) were treated and incubated at 37 °C for 24 hours. The media without any NPs were used as negative control, and each concentration was assayed in triplicate. The following equation was utilized to calculate cell viability (percentage):

$$Cell\ viability\ (\%) = \frac{(OD\ of\ control - OD\ of\ ZNO\ Np)}{OD\ of\ Control} \times 100$$

IC50 values were determined using the non-linear regression algorithm implemented by GraphPad.

The 50% growth inhibition concentration (IC50) was calculated by plotting the dose-response curve [42].

Analysis of DNA strand breakage and DNA damage

The alkaline comet assay was performed as described elsewhere [43]. The slides were precoated with agarose (0.5%) and air-dried at room temperature. Initially, the cells were collected by trypsinization, washed, and re-suspended in ice-cold PBS.

The re-suspended cells (10 µL) with low melting point agarose (100 µL) were added as the second layer and stored in a lysis buffer (4°C) for one hour [44, 45]. After lysis, the slides were performed electrophoresis in yellow light to prevent any DNA damage [46].

The slides were stained with EtBr (20 µg/mL) and analyzed in a fluorescence microscope (Carl Zeiss Optical Fluorescence Microscope). The comet images were analysed using open cometimage analysis software [43].

Statistical analysis

All the data in the experiments were analysed and expressed as the mean and standard deviation (SD) of two independent experiments. The data were analysed by Student's t-test or one-way analysis of variance using GraphPad Prism. A value of $P<0.05$ was considered to be statistically significant.

RESULTS AND DISCUSSION

UV–vis spectrophotometer

The ZnONPs showed the characteristic UV-vis absorption spectra at 300–380 nm, which revealed the proof for the synthesis of ZnONPs [47]. The UV-vis spectrum of GS- and CS-ZnONPs are shown in Fig 1.

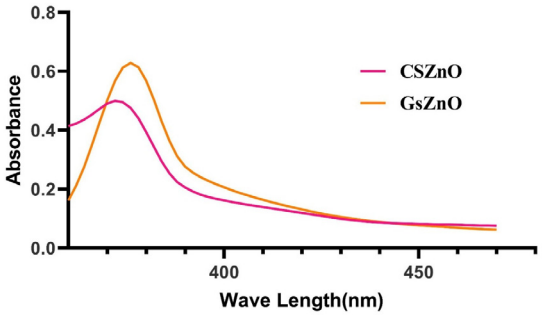

Fig 1. UV–Vis spectrum of chemically synthesized and green synthesized nanoparticles

The spectrum shows a characteristic sharp escalation in the absorption points at 372 nm and 378 nm for CS- and GS-ZnONPs. The absorption peak between 300-380 nm can be apportioned to the absorption spectra of ZnONPs due to the electron shifts to the conduction band from the valence band [1, 48]. Lack of any other peak in the range endorses that synthesized items are ZnONPs only, and a definite shift in the consumption onset was discernible in ZnONPs was synthesized with *S. trilobatum*. The spectrum of ZnO metal NPs will exhibit the property of SPR, which can shift in the wavelength due to the particle size or capping of phytochemicals from plant extract [40, 49, 50]. As described by earlier researchers, the SPR pattern strongly depends on the particle size, the capping or the stabilizing molecules which cover the surface of the NPs and the dielectric constant of the medium [51, 52]. The increase in the band gap energy from the CS- and GS-ZnONPs revealed the change of crystal structure of synthesized ZnONPs, which was in line with the results of Nithya and Kalyanasundharam, 2019 [52]. The ZnONPs

synthesized using *Eryngium foetidum* L., which revealed a characteristic ZnONPs peak at about 343 nm [53]. Besides, as reported by Ishwarya et al. (2018), ZnONPs were synthesized using *Ulva lactuca* seaweed extract exhibited a characteristic UV-vis absorption spectrum at 325 nm [54], whereas ZnONPs obtained from the root extract of *Scutellaria baicalensis* exhibited the absorption peak at 360 nm [33].

Scanning Electron Microscopy analysis (SEM)

The morphology of the ZnONPs was studied by SEM which were recorded at 30 kV from samples covered with a gold thin film with high vacuum mode.

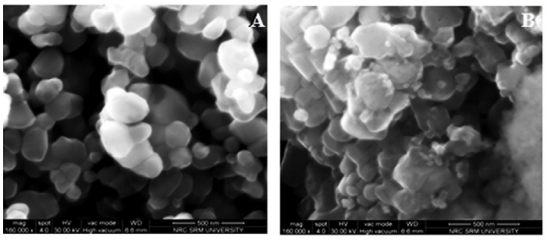

Fig 2. SEM image of (a) chemically synthesized ZnO nanoparticles, (B) green synthesized ZnO nanoparticles

Fig 2 shows the morphology of the CS- and GS-ZnONPs. From Fig 2, it is observed that the NPs were amorphous, spherical shaped with various sizes. Fig 2(A) clearly shows that NPs are not aggregated, but due to electrostatic and the surface energy, it is likely together. Fig 2(B), SEM image clearly shows that the surface of the ZnONPs is capped with the phytochemicals from the plant extract, acting as the stabilizing agents. The phytochemicals from *S. trilobatum* were responsible for the synthesis and bioreduction of the ZnONPs. As reported by Amir and Kumar (2004), the leaf extract of *S. trilobatum* contains phytochemicals such asalkaloids, triterpenoids, phytosterols, and saponins [55]. These phytochemicals and other constituents from *S. trilobatum* were responsible for the bioreduction, which acted as a capping agent to prevent aggregation of the synthesized ZnONPs. The SEM images of our earlier research have also shown the green synthesis methods utilizing the leaf extracts of *Mukia maderaspatna* [56], *Chrysopogon zizanioides* [39], and *M. umbellatum* [40] that were responsible for bioreduction and also showed no aggregation. Also, other studies confirmed the synthesis of ZnONPs utilizing the extracts of *Pithecellobium dulce* [57], *Codonopsis lanceolat* [58], *Juglans regia* [51], and *Scutellaria baicalensis* [33].

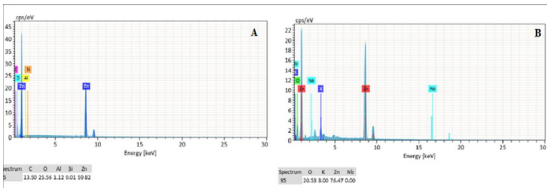

Fig 3. EDAX spectrum of (A) chemically synthesized ZnO nanoparticles, (B) green synthesized ZnO nanoparticles

Energy dispersive analysis spectroscopy (EDAX)

Fig 3 (A) shows the EDAX of CS-ZnONPs which discloses the presence of Zn and O that indicate the activity of pure ZnONPs. Tentatively, the stoichiometric mass percent of Zn and O was 59.8 and 25.56%, respectively. The sharpness of the peak corresponds to the elemental composition CS-ZnONPs. Fig 3 (B) shows the EDAX of GS-ZnONPs, which reveals the presence of Zn, O, and other Phyto-constituents confirming the purity of the synthesized ZnONPs.

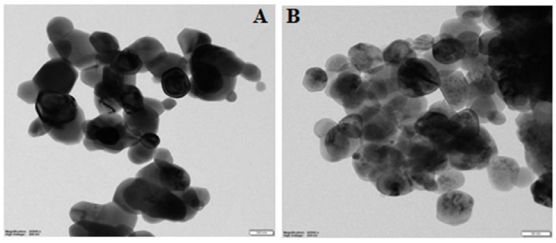

Fig 4. (A) TEM images of chemically synthesized ZnO nanoparticles, (B) TEM images of green synthesized ZnO nanoparticles

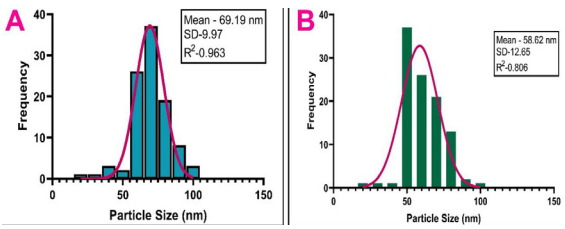

Fig 5. Particle size distribution graph of (A) chemically synthesized ZnO nanoparticles, (B) green synthesized ZnO nanoparticles

The contamination-free nanoparticle unveils the promising antimicrobial and antibiofilm activity.

Preferably, the anticipated stoichiometric mass percent of Zn and O was 80.3 and 19.7%, correspondingly. The GS-ZnONPs showed the elemental composition of Zn–76.47%, O–20.53%, and the other components were K–3.00%.

Transmission electron microscopy (TEM)

Fig 4(A) Shows the TEM image of the CS-ZnONPs. It is observed that CS-ZnONPs have uniform size shape with different morphology. Fig 4 (B) shows the TEM image of GS-ZnONPs which resemble a diffuse wave leaving from the crystal lattice plane. Fig 5 (A) shows the particle size distribution of CS-ZnONPs. The particle size and the distribution of the ZnONPs were determined using ImageJ Software.

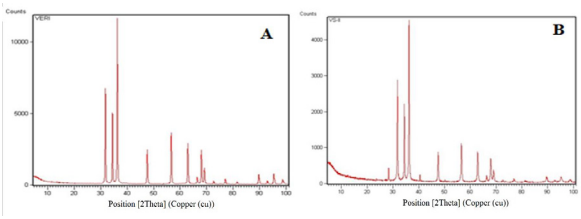

Fig 6. (A) XRD images of (A) chemically synthesized ZnO nanoparticles, (B) green synthesized ZnO nanoparticles

The particle size distribution of the CS-ZnONPs was of 20–100 nm range with an average particle size of 69.19 nm and the SD of 9.97 nm. Fig 5 (B) shows the particle size distribution of GS-ZnONPs. Similar to the chemical synthesized NPs, the particle size was determined using ImageJ Software. The particle size distribution of GS-ZnONPs ranges from 50-90 nm with the average particle size of 58.62 nm with the SD of 12.65 nm.

X-ray diffraction analysis (XRD)

Fig 6(A) represents the XRD pattern of CS-ZnONPs.

The peak intensity, full width half maximum, position, and width were analyzed from the XRD spectrum.

The diffraction peaks were positioned at 31.89º, 34.58º, 36.38º, 47.70º, 56.69º, 62.99º, 66.49º, 68.12º and 69.19º which have been indexed as phases of ZnONPs.

Table 1. Antimicrobial activity of various ZnO nanoparticles and S. trilobatum leaf extract at different concentrations against B. subtilis

Type	Zone of inhibition (mm)[ab]			
	50(mg/mL)	100(mg/mL)	200(mg/mL)	Standard Antibiotic[#]
CS-ZnO	15 ± 4.522	18 ± 1.2	20 ± 1.1	21.46 ± 1.32
GS-ZnO	19.6 ± 6.65	25.3 ± 2.081	28.6 ± 2.52	
Solanum trilobatum leaf extract	20.6 ± 7.57	19.66 ± 3.78	24 ± 1.732	

a The zone of inhibition represented has excluding the standard disk diameter of 6 mm
b The values represented are mean ± SD of three replicates.
The standard antibiotic utilized is Cefotaxime 30 µg (Hi-Media Laboratories, Mumbai, India)

Table 2. Antimicrobial activity of various ZnO nanoparticles and S. trilobatum leaf extract at different concentrations against E. coli

Type	Zone of inhibition (mm)[ab]			
	50(mg/mL)	100(mg/mL)	200(mg/mL)	Standard Antibiotic[#]
CS-ZnO	20 ± 4.35	23 ± 2.64	23.6 ± 0.213	17.9 ± 0.25
GS-ZnO	25.33 ± 1.15	25.6 ± 2.309	27.63 ± 0.577	
Solanum trilobatum leaf extract	14.6 ± 1.53	21.6± 0.577	22.6 ± 0.511	

a The zone of inhibition represented has excluding the standard disk diameter of 6 mm
b The value represented are mean ± SD of three replicates.
The Standard Antibiotic utilized is Tetracycline 30mcg (Hi-Media Laboratories, Mumbai, India)

Table 3. Antimicrobial activity of various ZnO nanoparticles and S. trilobatum leaf extract at different concentrations against K. pneumoniae

Type	Zone of inhibition (mm) [ab]			
	50(mg/mL)	100(mg/mL)	200(mg/mL)	Standard Antibiotic[#]
CS-ZnO	2 ± 0.5	26.67 ± 0.471	27.6 ± 0.94	
GS-ZnO	12 ± 4.5	22 ± 0.21	29.33 ± 0.816	14.9 ± 1.65
Solanum trilobatum leaf extract	21.6 ± 7.57	24.66 ± 3.78	25.5 ± 1.69	

a The zone of inhibition represented has excluding the standard disk diameter of 6 mm
b The values represented are the mean ± SD of three replicates.
The standard antibiotic utilized is Ampicillin 10 µg (Hi-Media Laboratories, Mumbai, India)

The diffraction peaks associated with the impurities were not perceived in the XRD pattern.

The line enlargement detected in the diffraction peaks was a typical observation, which proves that the synthesized materials are in the nanometer range. A similar observation was reported elsewhere [59].

There is no evidence of bulk residue materials, and other contamination in the CS-ZnONPs [60]. As reported by Talam et al., (2013), ZnONPs have exhibited the diffraction peaks located at 31.84°, 34.52°, 36.33°, 47.63°, 56.71°, 62.96°, 68.13°, and 69.18° have been strongly indexed as hexagonal quartzite phase of ZnO [61]. XRD analysis confirmed that CS-ZnONPs were small spherical shaped, crystalline in nature and were in good agreement with the characteristics of nano-sized particles as reported in the literature [62-64]. Fig 6 (B) represents the XRD pattern of the GS-ZnONPs. The leading diffraction peaks detected in the peaks matched to the Bragg reflections with 2θ values of 28.28º, 31.70º, 34.40º, 36.20º, 46.51º, 47.43º, 56.51º, 62.90º, and 66.49º which was related to the lattice plane of (1 0 0), (0 0 2), (1 0 1), (1 0 2), (1 1 0), (1 0 3), (1 1 2), (2 0 1),(0 0 4) suggesting the face-centered cubic crystal structure of the NPs. Our results were in line with the results of researchers reported earlier [35, 60, 65].

Antimicrobial activity

The antimicrobial activity of the CS- and GS-ZnONPs was investigated with three different concentrations (50, 100 and 200 mg/mL) against *B. subtilis, E. coli,* and *K. pneumoniae*. *B. subtilis* is Gram-positive, aerobic, rod-shaped bacteria, whereas *E. coli* and *K. pneumoniae* are Gram-negative, facultative anaerobic, rod-shaped bacteria. Table 1 shows the antimicrobial activity of CS- and GS-ZnONPs, and *Solanum trilobatum* leaf extract at different concentrations against *B. subtilis.* The GS-ZnONPs exhibited the higher zone of inhibition of 25.3±2.081 and 28.6±2.52 mm at 100 and 200 mg/mL, whereas the standard antibiotic Cefotaxime (30 µg) exhibited 21.46±1.32 mm. The presence of the inhibition zone clearly indicated that the *B. subtilis* cell wall membrane was disturbed and ZnONPs penetrated the cell and ultimately led to cell death. Table 2 shows the antimicrobial activity of CS- and GS-ZnONPs, and *S. trilobatum* leaf extract at different concentrations against *E. coli.* It is observed that GS-ZnONPs exhibited a higher zone of inhibition at all the concentrations.

The higher zone of inhibition of 27.63±0.577 mm at 200 mg/mL, whereas the standard antibiotic Tetracycline (30 µg) exhibited the zone of inhibition of 17.9±0.25 mm. From the morphology of nanoparticles, it was found that the GS-ZnONPs were spherical shaped, and the size of NPs were also smaller as compared to CS-ZnONPs.

It can be interpreted as the smaller NPs can easily penetrate the bacterial cell wall and show enhanced antimicrobial activity.

Table 3 shows the antimicrobial activity of CS- and GS-ZnONPs, and *S. trilobatum* leaf extract at different concentrations against *K. pneumoniae.* From the results, it is observed that GS-ZnONPs exhibited the higher zone of inhibition of 29.33±

0.816 mm at 200 mg/mL, whereas *S. trilobatum* leaf extract exhibited the higher zone of inhibition at lower concentrations. As reported by Elkady etal. (2015), ZnONPs at 30 mg/mL exhibited the inhibition zone of 23 mm against *B. subtilis*, and 32 mm against *E. coli* [66]. Rad et al., (2019) reported that ZnONPs from leaf extract of *Mentha pulegium* exhibited the maximum zone of inhibition at the concentration of 200 µg/mL [67].

The mechanism of antimicrobial property is related to the bactericidal effect of ZnO which prevents the bacterial growth wither by cell wall injury, pore development, seepage of ions and composites and cellular materials outside the membrane and causes the cell death. Our antimicrobial results were in line with the results of Darvishi *et al*., (2019) that reported green synthesized ZnONPs from walnut leaves with an antibacterial effect as compared to chemically synthesized ZnONPs [51].

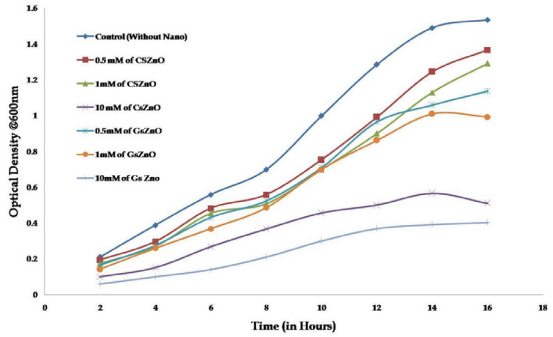

Fig 7. Time-dependent growth inhibition of E. coli with chemical and green synthesized ZnO nanoparticles. The value represented are mean ± SD of three independent experiments (N=3)

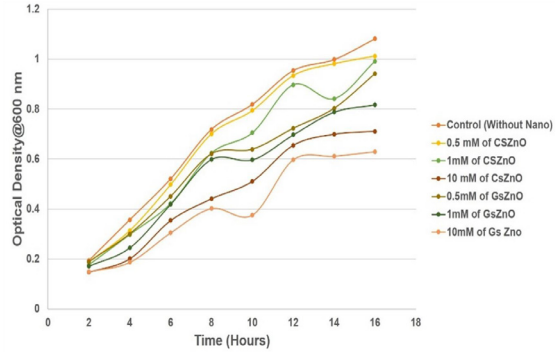

Fig 8. Time-dependent growth inhibition of S. aureus with chemical and green synthesized ZnO nanoparticles. The value represented are mean ± SD of three independent experiments (N=3)

Time-dependent growth inhibition assay

Time-dependent growth inhibition of *E. coli* with CS- and GS-ZnONPs is shown in Fig 7. The control cells without any NPs showed a higher optical density as compared to the CS- and GS-ZnONPs.

The increase in the concentration of CS- and/or GS-ZnONPs led to a decrease in the growth inhibition of *E. coli.* Even for 0.5 mM of CS- and GS-ZnONPs, the growth inhibition could be easily observed within 2 to 4 hr after the addition of NPs. The growth was declined entirely as compared to control within 10 hrs. From the results, it can be concluded that GS-ZnONPs exhibited higher growth inhibition as compared to CS-ZnONPs. Various researchers have reported that ZnONPs initially penetrated the cell membrane by damaging the membrane by direct or electrostatic interaction, thus induced the release of H2O2 [68, 69]. The released H2O2 initiated the production of reactive oxygen species, which caused alteration in the cellular internalization [70]. Time-dependent growth inhibition of *S. aureus*, with chemical and green synthesized ZnONPs is shown in Fig 8. The control cells without any NPs showed the higher optical density as compared to the CS- and GS-ZnONPs.

It could be seen that smaller ZnONPs has a much better antibacterial activity. Similar to the growth inhibition study of *E. coli,* the *S. aureus* encompassed the disruption of the cell membrane with a high rate of exponentiation of reactive oxygen species and eventually resulted in the death of microbes.

Kadiyala *et al*., (2018) carried out an extensive study on antimicrobial activity of ZnONPs against methicillin-resistant *S. aureus* and concluded that oxidative stress and dissolution of ZnO were adequate for the killing of methicillin-resistant *S. aureus* [71].

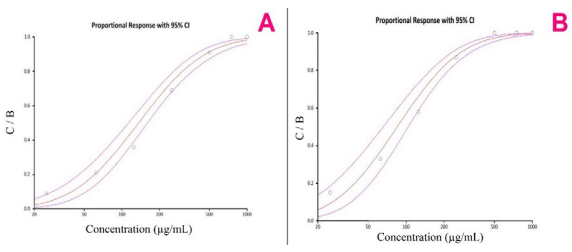

Fig 9. Inhibition curve for (A) chemical synthesized zinc oxide nanoparticle, (B) green synthesized zinc oxide nanoparticles on a human breast cancer cell line (MCF-7)

Anticancer Activity of ZnONPs

The anticancer activity of both CS- and GS-ZnONPs was investigated toward MCF-7 cells using MTT assay. Here untreated cells were utilized as a negative control. Fig 9(A) shows the inhibition curve for CS-ZnONPs. Fig 9(B) indicates the inhibition curve for GS-ZnONPs toward MCF-7 cells. This curve was obtained by plotting cell survival (percentage) versus drug concentration (µg/mL), and the cell growth inhibition (IC50) was calculated from curves. The rate constants and the fitted curve exhibited the dose-dependent decrease in cellular survival, and the curve exhibited the sigmoidal ailment that was characteristic of a competitive inhibitor. The IC50 for CS-ZnONPs was found at 136.16 µg/mL and for GS-ZnONPs was found at 85.05 µg/mL. The cytotoxic effects of GS-ZnONPs in MCF-7 cell lines were treated with concentrations of 0, 25, 62.5, 125, 250, 500, 750, and 1000 µg/mL and found the decreasing percentage of cell viability of 100, 85.21, 67.38, 42.03, 13.69, 2.01, 1.3, 1.01, respectively as shown in Fig 10.

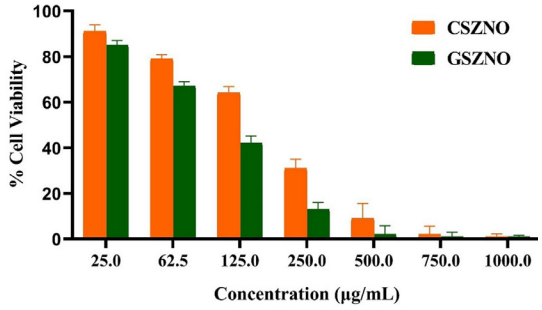

Fig 10. Cytotoxic effects of CS-ZnO and GS-ZnO on human breast cancer cell line (MCF-7). Each value represented are mean ± SD of three independent experiments (N=3)

The CS- and GS-ZnONPs exhibited dose-dependent inhibition against the proliferation of cancer cells. In the present study, as compared to CS-ZnONPs, the GS-ZnONPs exhibited higher cytotoxic effects on MCF-7 cell lines. Shobha *et al*., (2019) reported that ZnONPs initiated the cytotoxicity toward the MB–231 cells through the oxidative pressure by means of reactive oxygen species age [72]. The cytotoxicity study with pomegranate peel mediated synthesized ZnONPs were studied on CCD112 (colon cell line), while anticancer effects were evaluated on HCT116 (colorectal cancer cell line). The ZnONPs revealed the discriminatory toxicity toward colon cancer cells (HCT116) and proved non-toxic to normal cells (CCD112) [73]. The ZnONPs showed a discerning anticancer effect and showed no cytotoxicity in healthy cells. The ZnONPs induced the death of malignant tumor cells [34, 51, 74].

Analysis of DNA strand breakage and DNA damage

The comet assay was performed to evaluate the DNA damage on MCF-7 cells treated with 125, 250, and 500 µg/mL of CS- and GS-ZnONPs. The DNA damage (%) evaluated by comet assay on MCF-7 cells is shown in table 4. The nuclear morphology of the treated and untreated cells were utilized to calculate the DNA damage. The control cells showed only 3% of DNA damage, whereas the cells treated with 500 µg/mL exhibited the DNA damage of 48.11 and 57.2% for CS- and GS-ZnONPs. Similarly, herbal-mediated synthesized ZnONPs demonstrated the 7% DNA damage for the cells treated with 30 µg/mL of ZnONPs [75].

Table 4. Mean percentage of DNA damage by the comet assay in MCF-7 cells treated with different concentrations of chemically synthesized (CS-ZnO) and green synthesized (GC-ZnO) nanoparticles. Each value represented is mean ± SD of three independent experiments (N=3). A total of 100 nucleoids were analysed for each group to obtain % DNA in tail

Concentration	CS-ZnO	GS-ZnO
Negative Control	3.12±0.69	3.12±0.69
125 µg/mL	18.11 ±3.87	29.4±2.19
250 µg/mL	31.55±6.17	46.87±5.68
500 µg/mL	48.11±9.21	57.2±4.17

CONCLUSION

In this study, the ZnONPs were fabricated by both precipitation process and green synthesis method. The characterization studies demonstrated the successful synthesis of ZnONPs, and the XRD pattern endorsed the wurtzite structure. The EDAX analysis established the purity of ZnONPs. It was established that the purity of GS-Zn was 59.82%, and O was 25.56 %. In case of CS-ZnONPs, the purity of Zn was 76.47%, and O was 20.53%. The morphology of the synthesized

ZnONPs was found to be spherical with an average particle size of 34.75 nm in the CS-ZnO method, and 39.14 nm in the GS-ZnONPs. The internal structure of ZnONPs was found by TEM analysis. The cytotoxic effects of ZnONPs toward MCF-7 cells were evaluated in various concentrations and exhibited dose-dependent inhibition against the proliferation of malignancy of cancer cells. In the present study, as compared to CS-ZnONPs, the GS-ZnONPs exhibited higher cytotoxic effects toward MCF-7 cells. The antimicrobial analysis was performed to find the effectiveness of ZnONPs against pathogens such as *E. coli, K. pneumoniae,* and *B. subtilis* which were majorly causing infections in the urinary catheters. The enhanced antimicrobial activity of GS-ZnONPs obtained from *S. trilobatum* leaf extract were shown compared to CS-ZnONPs. It was concluded that GS-ZnONPs represented much enhanced anticancer and antibacterial activity compared to CS-ZnONPs.

ACKNOWLEDGMENTS

The authors wish to express their gratitude to Prof. Sasidharan, SRM Research Institute, SRM University, for TEM analysis. Karthiga Devi has expressed the sincere gratitude to AVIT who has permitted to carry the part of the research. This research did not receive any specific grant from funding agencies in the public, commercial, or not-for-profit sectors.

REFERENCES

1.Zak AK, Razali R, Majid WH, Darroudi M. Synthesis and characterization of a narrow size distribution of zinc oxide nanoparticles. Int J Nanomedicine. 2011; 6: 1399-1403.

2.Porter AL, Youtie J. How interdisciplinary is nanotechnology? J Nanopart Res. 2009; 11(5): 1023-1041.

3.Khan I, Saeed K, Khan I. Nanoparticles: Properties, applications and toxicities. Arabian J Chem. 2019; 12(7): 908-931.

4.Kim M, Lee J-H, Nam J-M. Plasmonic photothermal nanoparticles for biomedical applications. Adv Sci. 2019; 6(17): 1900471.

5.Segets D, Gradl J, Taylor RK, Vassilev V, Peukert W. Analysis of optical absorbance spectra for the determination of ZnO nanoparticle size distribution, solubility, and surface energy. ACS Nano. 2009; 3(7): 1703-1710.

6.Fan Z, Lu JG. Zinc oxide nanostructures: synthesis and properties. J Nanosci Nanotechnol. 2005; 5(10): 1561-1573.

7.Yang Y, Guo W, Zhang Y, Ding Y, Wang X, Wang ZL. Piezotronic effect on the output voltage of P3HT/ZnO micro/nanowire heterojunction solar cells. Nano Lett. 2011; 11(11): 4812-4817.

8.Yakimova R, Selegård L, Khranovskyy V, Pearce R, Lloyd Spetz A, Uvdal K. ZnO materials and surface tailoring for biosensing. Front Biosci. 2012; 4(1): 254-278.

9.Liu D, Wu W, Qiu Y, Yang S, Xiao S, Wang QQ, Ding L, Wang J. Surface functionalization of ZnO nanotetrapods with photoactive and electroactive organic monolayers. Langmuir. 2008; 24(9): 5052-5059.

10.Jiang J, Pi J, Cai J. The advancing of zinc oxide nanoparticles for biomedical applications. Bioinorg Chem Appl. 2018; 2018: 18.

11.Kolodziejczak-Radzimska A, Jesionowski T. Zinc oxide-from synthesis to application: a review. Materials. 2014; 7(4): 2833-2881.

12.Rane AV, Kanny K, Abitha VK, Thomas S. Chapter 5 - Methods for Synthesis of Nanoparticles and Fabrication of Nanocomposites. In: Mohan Bhagyaraj S, Oluwafemi OS, Kalarikkal N, Thomas S, editors. Synthesis of Inorganic Nanomaterials: Woodhead Publishing; 2018. p. 121-139.

13.Amendola V, Meneghetti M. Laser ablation synthesis in solution and size manipulation of noble metal nanoparticles. Phys. Chem. Chem. Phys. 2009; 11(20): 3805-3821.

14.Yang L. 2 - Nanotechnology-enhanced metals and alloys for orthopedic implants. In: Yang L, editor. Nanotechnology-Enhanced Orthopedic Materials. Oxford: Woodhead Publishing; 2015. p. 27-47.

15.Edelstein AS. Nanomaterials. In: Buschow KHJ, Cahn RW, Flemings MC, Ilschner B, Kramer EJ, Mahajan S, Veyssiere P. editors. Encyclopedia of Materials: Science and Technology. Oxford: Elsevier; 2001. p. 5916-5927.

16.Sols, Gels, and Organic Chemistry. In: Carter CB, Norton MG, editors. Ceramic Materials: Science and Engineering. New York, NY: Springer New York; 2007. p. 400-411.

17.Komarneni S. Nanophase materials by hydrothermal, microwave-hydrothermal and microwave-solvothermal methods. Curr Sci. 2003; 85(12): 1730-1734.

18.Parhi P, Kramer J, Manivannan V. Microwave initiated hydrothermal synthesis of nano-sized complex fluorides, KMF3 (K = Zn, Mn, Co, and Fe). J Mater Sci. 2008; 43(16): 5540-5545.

19.Latha PS, Kannabiran K. Antimicrobial activity and phytochemicals of Solanum trilobatum Linn. Afr J Biotechnol. 2006; 5(23): 2402-2404.

20.Premalatha S, Elumalai K, Jeyasankar A. Mosquitocidal properties of Solanum trilobatum L.(Solanaceae) leaf extracts against three important human vector mosquitoes (Diptera: Culicidae). Asian Pac J Trop Med. 2013; 6(11): 854-858.

21.Ramar M, Manikandan B, Marimuthu PN, Raman T, Mahalingam A, Subramanian P, Karthick S, Munusamy A. Synthesis of silver nanoparticles using Solanum trilobatum fruits extract and its antibacterial, cytotoxic activity against human breast cancer cell line MCF 7. Spectrochim Acta A Mol Biomol Spectrosc. 2015; 140: 223-228.

22.Xiang L, Wang Y, Yi X, He X. Steroidal alkaloid glycosides and phenolics from the immature fruits of Solanum nigrum. Fitoterapia. 2019; 137: 104268.

23.Rajkumar S, Jebanesan A. Oviposition deterrent and skin repellent activities of Solanum trilobatum leaf extract against the malarial vector Anopheles stephensi. J Insect Sci. 2005; 5: 15.

24.Ramakrishna S, Ramana K, Mihira V, Kumar BP. Evaluation of anti-inflammatory and analgesic activities of Solanum trilobatum. Linn Roots. Res J Pharm Biol Chem Sci. 2000; 2(1): 701-705.

25.Divyagnaneswari M, Christybapita D, Michael RD.

Enhancement of nonspecific immunity and disease resistance in Oreochromis mossambicus by Solanum trilobatum leaf fractions. Fish Shellfish Immunol. 2007; 23(2): 249-259.
26.Sahu J, Rathi B, Koul S, Khosa R. Solanum trilobatum (Solanaceae)-an overview. J Nat Rem. 2013; 13(2): 76-80.
27.Hong R, Pan T, Qian J, Li H. Synthesis and surface modification of ZnO nanoparticles. Chem Eng J. 2006; 119(2): 71-81.
28.Raoufi D. Synthesis and microstructural properties of ZnO nanoparticles prepared by precipitation method. Renewable Energy. 2013; 50: 932-937.
29.Arunachalam K, Arun L, Annamalai S, Arunachalam A. Potential anticancer properties of bioactive compounds of Gymnema sylvestre and its biofunctionalized silver nanoparticles. Int J Nanomed. 2015; 10: 31-41.
30.Arunachalam KD, Annamalai SK, Arunachalam AM. One step green synthesis of phytochemicals mediated gold nanoparticles from Aegle marmales for the prevention of urinary catheter infection. Int Jounal Pharm Pharm Sci. 2014; 6: 700-706.
31.Elavazhagan T. Memecylon edule leaf extract mediated green synthesis of silver and gold nanoparticles. Int J Nanomed. 2011; 6: 1265-1278.
32.Gawade V, Gavade N, Shinde H, Babar S, Kadam A, Garadkar K. Green synthesis of ZnO nanoparticles by using Calotropis procera leaves for the photodegradation of methyl orange. J Mater Sci: Mater Electron. 2017; 28(18): 14033-14039.
33.Chen L, Batjikh I, Hurh J, Han Y, Huo Y, Ali H, Li JF, Rupa EJ, Ahn JC, Mathiyalagan R, Yang DC. Green synthesis of zinc oxide nanoparticles from root extract of Scutellaria baicalensis and its photocatalytic degradation activity using methylene blue. Optik. 2019; 184: 324-329.
34.Sharmila G, Thirumarimurugan M, Muthukumaran C. Green synthesis of ZnO nanoparticles using Tecoma castanifolia leaf extract: Characterization and evaluation of its antioxidant, bactericidal and anticancer activities. Microchem J. 2019; 145: 578-587.
35.Santhoshkumar J, Kumar SV, Rajeshkumar S. Synthesis of zinc oxide nanoparticles using plant leaf extract against urinary tract infection pathogen. Resour-Effic Technol. 2017; 3(4): 459-465.
36.Gunalan S, Sivaraj R, Rajendran V. Green synthesized ZnO nanoparticles against bacterial and fungal pathogens. Prog Nat Sci: Mater Int. 2012; 22(6): 693-700.
37.Dipankar C, Murugan S. The green synthesis, characterization and evaluation of the biological activities of silver nanoparticles synthesized from Iresine herbstii leaf aqueous extracts. Colloids Surf, B. 2012; 98: 112-119.
38.Arunachalam KD, Arun LB, Annamalai SK, Arunachalam AM. Biofunctionalized gold nanoparticles synthesis from Gymnema sylvestre and its preliminary anticancer activity. Int J Pharm Pharm Sci. 2014; 6(4): 423-430.
39.Arunachalam K, Annamalai S. Chrysopogon zizanioides aqueous extract mediated synthesis, characterization of crystalline silver and gold nanoparticles for biomedical applications. Int J Nanomed. 2013; 8: 2375-23784.
40.Arunachalam K, Annamalai S, Hari S. One-step green synthesis and characterization of leaf extract-mediated biocompatible silver and gold nanoparticles from Memecylon umbellatum. Int J Nanomed. 2013; 8: 1307-1315.
41.Mosmann T. Rapid colorimetric assay for cellular growth and survival: Application to proliferation and cytotoxicity assays. J Immunol Methods. 1983; 65(1): 55-63.
42.Boroumand Moghaddam A, Moniri M, Azizi S, Abdul Rahim R, Bin Ariff A, Navaderi M, Mohamad R. Eco-friendly formulated zinc oxide nanoparticles: induction of cell cycle arrest and apoptosis in the MCF-7 cancer cell line. Genes. 2017; 8(10): 281.
43.Annamalai SK, Arunachalam KD. Uranium (238U)-induced ROS and cell cycle perturbations, antioxidant responses and erythrocyte nuclear abnormalities in the freshwater iridescent shark fish Pangasius sutchi. Aquat. Toxicol. 2017; 186: 145-158.
44.Arunachalam K, Annamalai S, Kuruva J. In-vivo evaluation of hexavalent chromium induced DNA damage by alkaline comet assay and oxidative stress in Catla catla. Am J Environ Sci. 2013; 9(6): 470-482.
45.Rojas E, Lopez M, Valverde M. Single cell gel electrophoresis assay: methodology and applications. J Chromatogr B: Biomed Sci Appl. 1999; 722(1-2): 225-254.
46.Annamalai SK, Arunachalam KD. Uranium induced ROS and its antioxidant defense molecules, genotoxicity assessment in iridescent shark (Pangasius sutchi). In Proceedings of the international conference on radiation biology: frontiers in radiobiology-immunomodulation, countermeasures and therapeutics: abstract book, souvenir and scientific programme 2014.
47.Yuan R, Xu H, Liu X, Tian Y, Li C, Chen X, Su S, Perelshtein I, Gedanken A, Lin X. Zinc-doped copper oxide nanocomposites inhibit the growth of human cancer cells through reactive oxygen species-mediated NF-κB activations. ACS Appl Mater Interfaces. 2016; 8(46): 31806-31812.
48.Goh EG, Xu X, McCormick PG. Effect of particle size on the UV absorbance of zinc oxide nanoparticles. Scr Mater. 2014; 78-79: 49-52.
49.Jamdagni P, Khatri P, Rana JS. Green synthesis of zinc oxide nanoparticles using flower extract of Nyctanthes arbor-tristis and their antifungal activity. J King Saud Univ, Sci. 2018; 30(2): 168-175.
50.Halawani EM. Rapid biosynthesis method and characterization of silver nanoparticles using Zizyphus spina christi leaf extract and their antibacterial efficacy in therapeutic application. J Biomater Nanobiotechnol. 2016; 8(1): 22-35.
51.Darvishi E, Kahrizi D, Arkan E. Comparison of different properties of zinc oxide nanoparticles synthesized by the green (using Juglans regia L. leaf extract) and chemical methods. J Mol Liq. 2019; 286: 110831.
52.Nithya K, Kalyanasundharam S. Effect of chemically synthesis compared to biosynthesized ZnO nanoparticles using aqueous extract of C. halicacabum and their antibacterial activity. OpenNano. 2019; 4: 100024.
53.Begum S, Ahmaruzzaman M, Adhikari PP. Ecofriendly bio-synthetic route to synthesize ZnO nanoparticles using Eryngium foetidum L. and their activity against pathogenic bacteria. Mater Lett. 2018; 228: 37-41.
54.Ishwarya R, Vaseeharan B, Kalyani S, Banumathi B, Govindarajan M, Alharbi NS, Kadaikunnan S, Al-Anbr MN, Khaled JM, Benelli G. Facile green synthesis of zinc oxide nanoparticles using Ulva lactuca seaweed extract and evaluation of their photocatalytic, antibiofilm and insecticidal activity. J Photochem Photobiol, B. 2018; 178:

249-258.
55.Amir M, Kumar S. Possible industrial applications of genus Solanum in twentyfirst century: A review. J Sci Ind Res. 2004; 63(2): 116-124.
56.Devi GK, Sathishkumar K. Synthesis of gold and silver nanoparticles using Mukia maderaspatna plant extract and its anticancer activity. IET Nanobiotechnol. 2016; 11(2): 143-151.
57.Madhumitha G, Fowsiya J, Gupta N, Kumar A, Singh M. Green synthesis, characterization and antifungal and photocatalytic activity of Pithecellobium dulce peel–mediated ZnO nanoparticles. J Phys Chem Solids. 2019; 127: 43-51.
58.Lu J, Ali H, Hurh J, Han Y, Batjikh I, Rupa EJ, Anandapadmanaban G, Park JK, Yang DC. The assessment of photocatalytic activity of zinc oxide nanoparticles from the roots of Codonopsis lanceolata synthesized by one-pot green synthesis method. Optik. 2019; 184: 82-89.
59.Mohan AC, Renjanadevi B. Preparation of zinc oxide nanoparticles and its characterization using scanning electron microscopy (SEM) and X-ray diffraction (XRD). Procedia Technol. 2016; 24: 761-766.
60.Bindu P, Thomas S. Estimation of lattice strain in ZnO nanoparticles: X-ray peak profile analysis. J Theor App Phys. 2014; 8(4): 123-134.
61.Talam S, Karumuri SR, Gunnam N. Synthesis, characterization, and spectroscopic properties of ZnO nanoparticles. ISRN Nanotechnol. 2012; 2012: 6.
62.Kumar SS, Venkateswarlu P, Rao VR, Rao GN. Synthesis, characterization and optical properties of zinc oxide nanoparticles. Int Nano Lett. 2013; 3(1): 30.
63.Fu Y-S, Du XW, Kulinich SA, Qiu JS, Qin WJ, Li R, Sun J, Liu J. Stable aqueous dispersion of ZnO quantum dots with strong blue emission via simple solution route. J Am Chem Soc. 2007; 129(51): 16029-16033.
64.Singh AK. Synthesis, characterization, electrical and sensing properties of ZnO nanoparticles. Adv Powder Technol. 2010; 21(6): 609-613.
65.Suresh J, Pradheesh G, Alexramani V, Sundrarajan M, Hong SI. Green synthesis and characterization of zinc oxide nanoparticle using insulin plant (Costus pictus D. Don) and investigation of its antimicrobial as well as anticancer activities. Adv Nat Sci: Nanosci Nanotechnol. 2018; 9(1): 015008.
66.Elkady MF, Shokry Hassan H, Hafez EE, Fouad A. Construction of zinc oxide into different morphological structures to be utilized as antimicrobial agent against multidrug resistant bacteria. Bioinorg Chem Appl. 2015; 2015: 20.
67.Rad SS, Sani AM, Mohseni S. Biosynthesis, characterization and antimicrobial activities of zinc oxide nanoparticles from leaf extract of Mentha pulegium (L.). Microb Pathog. 2019; 131: 239-245.
68.Zhang L, Jiang Y, Ding Y, Povey M, York D. Investigation into the antibacterial behaviour of suspensions of ZnO nanoparticles (ZnO nanofluids). J Nanopart Res. 2007; 9(3): 479-489.
69.Zhang L, Jiang Y, Ding Y, Daskalakis N, Jeuken L, Povey M, O'Neill AJ, York DW. Mechanistic investigation into antibacterial behaviour of suspensions of ZnO nanoparticles against E. coli. J. Nanopart. Res. 2010; 12(5): 1625-1636.
70.Reddy LS, Nisha MM, Joice M, Shilpa P. Antimicrobial activity of zinc oxide (ZnO) nanoparticle against Klebsiella pneumoniae. Pharm Biol. 2014; 52(11): 1388-1397.
71.Kadiyala U, Turali-Emre ES, Bahng JH, Kotov NA, VanEpps JS. Unexpected insights into antibacterial activity of zinc oxide nanoparticles against methicillin resistant Staphylococcus aureus (MRSA). Nanoscale. 2018; 10(10): 4927-4939.
72.Shobha N, Nanda N, Giresha AS, Manjappa P, Sophiya P, Dharmappa KK, Nagabhushana BM. Synthesis and characterization of Zinc oxide nanoparticles utilizing seed source of Ricinus communis and study of its antioxidant, antifungal and anticancer activity. Mater Sci Eng, C. 2019; 97: 842-850.
73.Mohamad Sukri SNA, Shameli K, Mei-Theng Wong M, Teow S-Y, Chew J, Ismail NA. Cytotoxicity and antibacterial activities of plant-mediated synthesized zinc oxide (ZnO) nanoparticles using Punica granatum (pomegranate) fruit peels extract. J Mol Struct. 2019; 1189: 57-65.
74.Anitha R, Ramesh KV, Ravishankar TN, Sudheer Kumar KH, Ramakrishnappa T. Cytotoxicity, antibacterial and antifungal activities of ZnO nanoparticles prepared by the Artocarpus gomezianus fruit mediated facile green combustion method. J Sci: Adv Mater Devices. 2018; 3(4): 440-451.
75.Ahmar Rauf M, Oves M, Ur Rehman F, Rauf Khan A, Husain N. Bougainvillea flower extract mediated zinc oxide's nanomaterials for antimicrobial and anticancer activity. Biomed Pharmacother. 2019; 116: 108983.